Separation and Purification Technology 68 (2009) 83–89

Contents lists available at ScienceDirect

Separation and Purification Technology

journal homepage: www.elsevier.com/locate/seppur

Effect of synthesis conditions on photocatalytic activities of nanoparticulate TiO_2 thin films

Lei Sun[a,d], Taicheng An[a,*], Shungang Wan[a,d], Guiying Li[a], Ningzhong Bao[b], Xiaohong Hu[c], Jiamo Fu[a], Guoying Sheng[a]

[a] State Key Laboratory of Organic Geochemistry and Guangdong Key Laboratory of Environmental Resources Utilization and Protection, Guangzhou Institute of Geochemistry, Chinese Academy of Sciences, Guangzhou 510640, China
[b] Center for Materials for Information Technology, The University of Alabama, Tuscaloosa, AL 35487, USA
[c] Sciences School, Foshan University, Guangdong, Foshan 528000, China
[d] Graduate School of Chinese Academy of Sciences, Beijing 100049, China

ARTICLE INFO

Article history:
Received 11 January 2009
Received in revised form 6 April 2009
Accepted 13 April 2009

Keywords:
TiO_2 thin film
Preparation parameters
Sol–gel method
Design of experiments (DOE)
Photocatalytic activity

ABSTRACT

In the present study, design of experiments (DOE) was used to find an optimal combination for the factors affecting the preparation, morphology and catalytic activity of nano-crystalline TiO_2 thin films synthesized by sol–gel method. Nine TiO_2 thin films were prepared onto indium–tin oxide (ITO) substrates by changing four operating parameters at three levels. The four operating parameters are the volume of 20% acetic acid aqueous solution, the volume of co-solvent alcohol, the amount of template reagent (triblock copolymer Pluronic P123), and the calcination temperature. The resulting films were characterized by X-ray diffraction (XRD), field emission-scanning electron microscopy (FE-SEM), atomic force microscopy (AFM), and Fourier transform-infrared (FT-IR) spectra. The results of DOE are examined by both the direct observation analysis (also called range analysis) and the analysis of variance (ANOVA) with 90 or 95% confidence intervals. The parameter settings have been optimized as the combination of precursor solution constitution of $Ti(OC_4H_9)_4$/20%HAC/EtOH/P123 (2 g/15 ml/8 ml/1.1 g), calcination temperature of 450 °C, calcination time of 3 h, and air reaction atmosphere. The thin film prepared under the optimal combination consists of ordered compact anatase nanoparticles with an average grain size of approximately 17.2 nm and an average roughness of 3.653 nm. The 1-h photodegradation efficiency of methyl orange (MO) in aqueous solution and toluene in gaseous phase is 98.9 and 100%, respectively. The factor analysis results of degradation efficiencies show that the calcinations temperature plays an important role in determining the photocatalytic activity of the prepared TiO_2 thin film. Furthermore, the surface morphology-dependent photocatalytic activity of the prepared thin films was also found.

1. Introduction

Nano-crystalline TiO_2 thin films have been intensively investigated in recent years, because of their different potential applications including air purification [1–5], water purification or water treatment [6–9], sterilization or disinfections [10,11], solar energy cells [12,13] and gas sensors [14]. TiO_2 films can be synthesized by many techniques, such as sol–gel method [15], chemical vapor deposition [16], reactive sputtering [17], and cathodic arc deposition [18]. Among these techniques, the sol–gel method is one of the simplest and cost-effective synthetic technique with several advantages, such as low processing temperature, homogeneity, and easy formation of large-area coating on substrates [19].

The optimal synthetic conditions for the preparation of TiO_2 thin film by sol–gel method have been reported. Zhao et al. investigated many synthetic conditions, such as the amount of surfactant template, the amount of hydrolysis retardant acetylacetone, the sol aging time, the pH value of sol, and the calcination temperature [20]. Liu et al. also used the optimized $Ti(OC_4H_9)_4$–P123–EtOH–HCl system for the preparation of nano-crystalline TiO_2 thin films [21]. Zhang et al. studied the effect of the molecular weight of ethylene glycol (PEG) and the molar ratio of the structure-directing agent in the sol–gel method [22], which is similar to our hydrothermally assisted sol–gel method by using P123 [23] and PEG [6] as templates. Thus, we can conclude that a number of batched experiments are required for determining an optimal synthetic condition for preparing thin films. However, almost all the reported research works only investigated the influential factors individually, and did not consider other preparation variables and the relationship among them. If many factors were individually analyzed, especially

* Corresponding author. Tel.: +86 20 85291501; fax: +86 20 85290706.
E-mail address: antc99@gig.ac.cn (T. An).

1383-5866/$ – see front matter © 2009 Elsevier B.V. All rights reserved.
doi:10.1016/j.seppur.2009.04.011

Table 1
Assignment of L9 orthogonal array.

Run no.	Factor A. 20% HAC (ml)	Factor B. EtOH (ml)	Factor C. P123 (g)	Factor D. Calcination temperature (°C)
1#	15	6	0.5	350
2#	15	8	1.1	450
3#	15	10	1.7	550
4#	25	6	1.1	550
5#	25	8	1.7	350
6#	25	10	0.5	450
7#	35	6	1.7	450
8#	35	8	0.5	550
9#	35	10	1.1	350

in a complicated system for thin film preparation [24], the experimental efficiency is significantly low. Therefore, the strategy to develop an efficient experimental design for determining optimal synthetic conditions of TiO_2 thin film is required.

The design of experiments (DOE) is an alternative approach to mass experimental processes. This statistic method is capable of solving many complicated synthesis problems with multiple variables and reducing the number of time-consuming experiments from economic and scientific viewpoints [25]. Wu et al. [24] recently reported the parameter optimization by the DOE for the sol–gel fabrication of hybrid catalysts on porous medium with the use of a fixed precursor sol recipe. However, the optimization of the precursor sol is also very important for improving the photocatalytic activity, because the activity of TiO_2 thin film is determined by both the coating procedure and the preparation recipe of the precursor sol. However, no systematic research work both on the optimization of affecting factors for the preparation of the precursor sol and on the relationship between the photocatalytic activity of the prepared TiO_2 thin film and various affecting parameters have not been studied until now.

In the present study, four controlling factors at three levels were applied to find out the optimal combination of synthetic parameters for the sol–gel preparation of photocatalytically active TiO_2 thin film onto ITO according to assignment of L9 orthogonal array. The surface morphology-dependent photocatalytic activity of TiO_2 thin films was also investigated by performing liquid-phase photocatalytic degradation of methyl orange (MO) and gas-phase photocatalytic degradation of toluene.

2. Experiment

2.1. L9 orthogonal array

Base on our pervious studies [23], four controlling factors at three levels were selected to investigate the optimal parameter settings. Table 1 presents the L9 orthogonal array for the preparation of TiO_2 thin films. The three levels for controlling factors are 15, 25, and 35 ml for the factor A, the volume of 20% acetic acid aqueous solution; 6, 8, and 10 ml for the factor B, the volume of ethanol used as co-solvent; 0.5, 1.1, and 1.7 g for the factor C, the amount of triblock copolymer, Pluronic P123 (*M*av = 5800, designated as $EO_{20}PO_{70}EO_{20}$); and 350, 450, and 550 °C for the factor D, the calcination temperature.

2.2. Preparation and characterization of TiO_2 thin films

The indium–tin oxide (ITO) conducting glass (80–100 Ω per square, Shenzhen, China) was cut into 12 cm × 5.7 cm pieces. All the pieces were cleaned by ultrasonic rinse in a detergent solution for 30 min, in acetone and chromate lotion for 10 s, and rinsed with distilled water, and then air-drying. A series of TiO_2 thin films were prepared via the sol–gel method according to the designed orthogonal array. For a typical synthesis, 2 g of titanium butoxide ($Ti(OC_4H_9)_4$, TBT) was added dropwise to 20% (v/v) acetic acid aqueous solution under vigorous magnetic stirring. The well-mixed solution was sealed and kept stirring at room temperature for 3 h to obtain the solution A. In a separated beaker, triblock copolymer, Pluronic P123 was dissolved in ethanol thoroughly under vigorous magnetic stirring to obtain the solution B. The solution B was slowly added to the solution A, and the mixed solution was continuously stirring at ambient temperature for another 3 h. The resultant sol was homogenized by ultrasonic vibration for 5 min and then aged at room temperature for 24 h. The cleaned ITO slide was dip-coated with the prepared TiO_2 colloidal solution, and then dried at 120 °C for 10 min. Such coating procedure was repeated four times. Finally, the as-synthesized thin films were calcined in a muffle furnace at a given temperature for 3 h at a heating rate of 2 °C/min in air. Nine prepared films are defined as film 1#–9#, respectively.

The structure of typical films was investigated by Nicolet 330 Fourier transform-infrared (FT-IR) at the wave number range of 0–4500 cm^{-1}. The crystal phase and the crystallite size of all the obtained TiO_2 thin film were measured by Bruker D8 Advance X-ray diffraction (XRD). All the samples were measured in the angular range of 10–60° (2θ) at a scan rate of 2°/min with the using of Cu Kα radiation (λ = 0.154056 nm) operating at 40 kV and 40 mA. Thermal field emission environmental scanning electron microscope (FE-SEM, Quanta 400 FEG) under high vacuum mode was used to observe the morphology of the film photocatalysts. The surface morphology was further studied by atomic force microscopy (AFM) at tapping mode with a Nanoscope III Digital-VEECO (E type scanner, 512 × 512 pixels, with scanned size 500 nm × 500 nm).

2.3. Characterization of photocatalytic activity

Photocatalytic degradation of methyl orange (MO) in aqueous solution was conducted in a 105 ml quadrate quartz reactor (12.5 cm × 1.2 cm × 7.0 cm) with air aeration from a pump at an air flow rate of 0.15 m^3/h. The initial concentration of MO was 10.0 mg/l. A 125 W high-pressure mercury lamp with a maximum emitting radiation of 365 nm (GGZ125, Shanghai Yaming Lighting Co., Ltd.) was used as the UV-light source, placing parallel to the quartz reactor. The distance between the surface of the TiO_2 thin film photocatalyst and the lamp was 20 cm, and the average intensity of the UV-light is about 2.2 mW cm^{-2}. One piece of the TiO_2/ITO film was put into 90 ml MO aqueous solutions under aeration mixing. The photocatalytic degradation of MO was carried out for 60 min under the UV irradiation. Prior to irradiation, all the reactions were kept aerating in the dark for 15 min to reach the adsorption equilibrium of MO onto the TiO_2 films.

Photocatalytic degradation of gaseous toluene at the gas–solid interface was carried out in a sealed 5 l Pyrex glass reactor. Two identical prepared TiO_2/ITO films were installed facing to the UV source placed in the centre of double-walled quartz cylinder. In all the experiments, the reaction temperature was kept at room temperature by a continuous circulation of cooling water in the quartz glass jacket around the light source. The light intensity was maintained at an average 5.3 mW cm^{-2} in all the measurements. A minitype fan stirrer placed at the bottom of the reactor was used as the air blender for reaction gas, which ensures effective transfer of the gaseous molecules in the reactor. The liquid toluene and a small fraction of water were injected into the batch reactor, and then allowed to vapor, mix, and reach the gas–solid adsorption equilibrium after the reactor was flushed and filled with pressured air. The equilibrium concentration of toluene was about 0.6 mg/l and the relative humidity was ca. 45%. Once the concentration of toluene was stabilized, the photocatalytic degradation of toluene was started by tuning on the UV lamp.

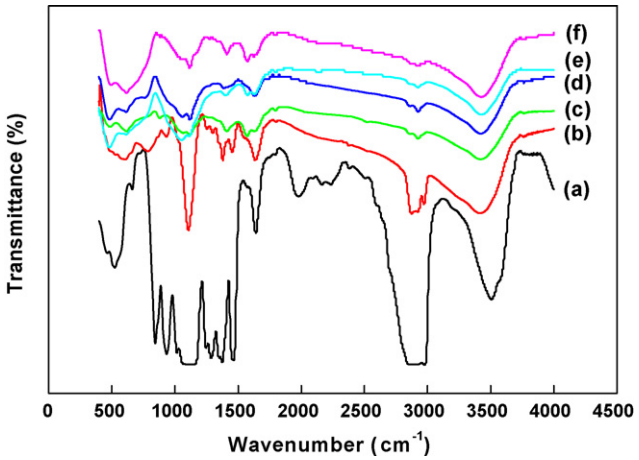

Fig. 1. FT-IR spectra of (a) P123 and the 2# TiO_2 thin film calcined at (b) 150, (c) 250, (d) 350, (e) 450, and (f) 550 °C.

2.4. Analytical method

The concentration of MO was analyzed by using an UV–vis spectroscopy (Thermo Spectronic Helios α series, USA) at its maximum absorption wavelength of 463 nm. The absorbency values were converted to the concentration by using the calibration curves. The photocatalytic degradation efficiencies of MO were calculated by comparing the loss concentration at 1 h illumination with the initial concentration. A gas chromatograph (HP 5890, Series II, equipped with a split/splitless injector and a flame ionization detector) and a HP-5 MS capillary column (0.32 mm × 0.25 μm × 30 m, Agilent Technologies) were used to analyze the concentration of gaseous toluene. The injector temperature and the detector temperature were set at 200 and 230 °C, respectively. 300 μl reacted gas was taken at given intervals for the GC analysis, using a 500 μl gas-tight locking syringe (Agilent, Australia). The column temperature was maintained at 40 °C for 2 min, and then increased to final 80 °C at a rate of 5 °C/min. The chromatographic peak areas were converted to the concentration values by using calibration curves based on the standard compounds.

3. Results and discussion

3.1. Characterization of TiO_2 thin films

3.1.1. FT-IR spectra

The chemical composition of the prepared films calcined at different temperatures and the elimination of organics template during post-heat treatment was investigated by FT-IR (Fig. 1), using 2# film as an example. The FT-IR spectra of the organic template P123 and the thin films prepared at calcination temperatures ranging from 150 to 550 °C were presented in Fig. 1a–f. As shown in Fig. 1a, the strong peaks in the range of 2850–2930 cm^{-1} and at around 1100 cm^{-1} are assigned to the C–H and C–O–C stretching vibration of P123, respectively [20]. As indicated by Fig. 1b–f, with increasing the calcination temperature, the strong infrared absorption bands appearing at 2850–2930 cm^{-1} disappeared, and the peak at 1100 cm^{-1} becomes weaker, specially for the calcination temperature above 250 °C, which is due that the organic template is partially removed. Meanwhile, a wide peak at 400–1000 cm^{-1} identified as the lattice vibrations of Ti–O–Ti bonds becomes stronger with increasing the calcined temperature. Another strong peak at 3500–3600 cm^{-1} in profile of P123 (Fig. 1a) was identical as the presence of hydroxyl groups. However, this peak is observed in the FT-IR profiles of all the samples, which is due to the existence of residual OH groups bonded with Ti in samples [26].

3.1.2. XRD patterns

Generally, the TiO_2 photocatalysts with good crystallinity and small particle size exhibit good photocatalytic activity [27]. XRD patterns were used to investigate the phase structure and the phase composition of the prepared TiO_2 films. The XRD patterns of nine TiO_2 thin films prepared from L9 orthogonal array and the blank ITO substrate were shown in Fig. 2. A broadening peak at 20–40° is caused by the amorphous structure of silica constitute of the ITO glass substrate [28]. The strongest peak appearing at 25.32° and a weak peak appearing at 48.07° can be assigned to the (1 0 1) and (2 0 0) peaks of anatase TiO_2 films, respectively. It is noteworthy that the (1 0 1) peak intensity for 1# and 2# films is higher than those of others, indicating that 1# and 2# films have good crystallinity. The amount of loaded TiO_2 photocatalyst from 1# to 9# films are 0.122, 0.211, 0.040, 0.057, 0.065, 0.105, 0.093, 0.047 and 0.033 mg/cm^2, respectively. 1# and 2# have much higher TiO_2 loading amount than other films. Moreover, the average grain size of TiO_2 nanocrystals from 1# to 9# films, calculated from the broadening XRD peak (1 0 1) of anatase phase according to Scherrer formula, is 38.7, 17.2, 18.2, 15.5, 12.0, 14.2, 14.3, 14.9 and 12.3 nm, respectively. The particle size of 1# film is largest one.

3.1.3. FE-SEM observation

Fig. 3 shows FE-SEM images of ITO glass and representative TiO_2 thin films marked with 2#, 3# and 7#. The ITO substrate (Fig. 3a) has very smooth surface. However, nanoparticle agglomerates, as shown in Fig. 3b–d, are observed on the ITO substrate after coating with different amount of TiO_2. A few isolated nanoparticle agglomerates scattered onto the ITO glass surface were observed on 3# film (Fig. 3c). On the contrary, many nanoparticle agglomerates are uniformly coated on the ITO surface for 2# film (Fig. 3b) and 7# film (Fig. 3d). However, the packing density of nanoparticle agglomerates for 2# film is larger than that of 7# film. The average particle sizes of TiO_2 nanoparticles for 2#, 3# and 7# films are all less than 20 nm, which agrees with the average grain sizes calculated for the XRD patterns.

3.1.4. AFM images

In order to fully understand the dependence of the surface morphologies on the parameters optimized by DOE, AFM was also

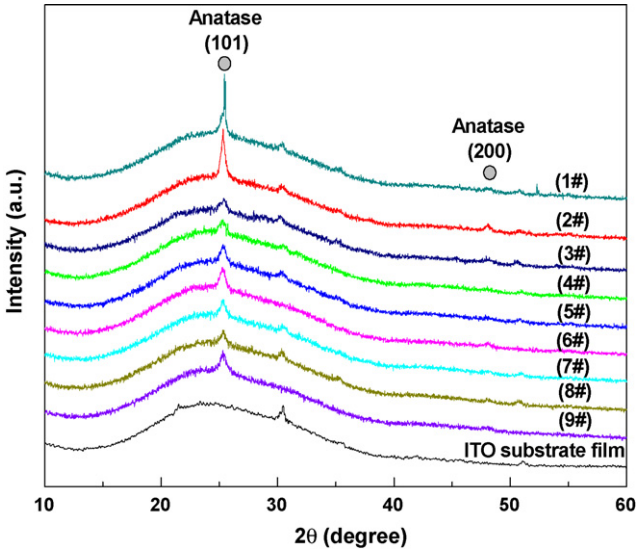

Fig. 2. XRD patterns of ITO substrate and TiO_2 thin films prepared on the ITO.

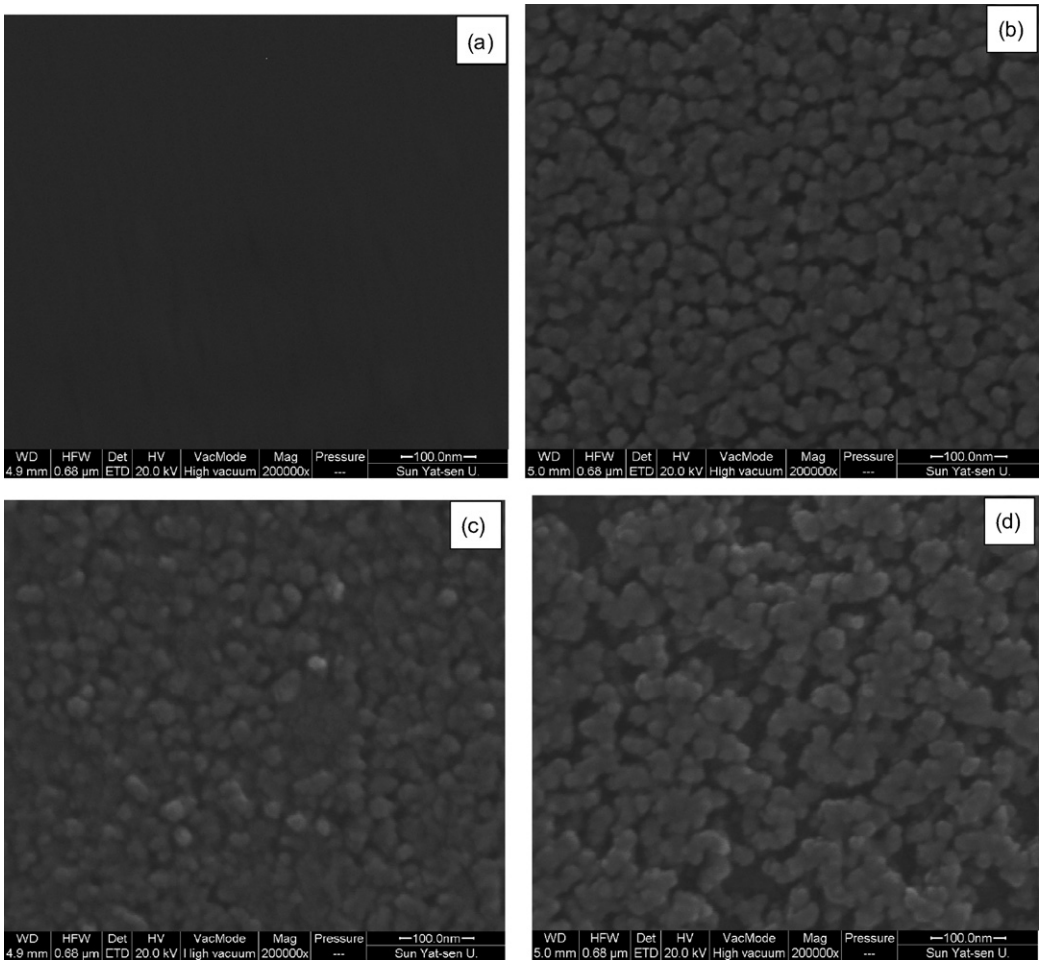

Fig. 3. FE-SEM images of (a) ITO substrate and representative TiO_2 films of (b) 2# film, (c) 3# film, and (d) 7# film.

employed to observe the surface and texture features of the synthesized TiO_2 films. Three-dimensional AFM images of 2# and 3# films are shown in Fig. 4a and b, respectively. Both of the TiO_2 films consist of interconnected spherical nanoparticles. The surfaces of the 2# film is composed of uniform and pretty dense spherical grain-like structures at the same altitude, while the 3# film is not smooth and exhibits concavo-convex structures of nanoparticle agglomerates. The average grain sizes, calculated from the related AFM images, of TiO_2 particles are about 20.79 nm for 2# film and 14.75 nm for 3# film, agreeing with the results calculated form related X-ray patterns (Fig. 2) and FE-SEM images (Fig. 3). In addition to the grain size of TiO_2, the maximum height (Rmax), the average roughness value (Ra), and the root mean square roughness (Rms) of surface features are also essential parameters for determining the photocatalytic activity [29]. An Rmax of 15.922 nm, with a Ra of 3.653 nm and Rms of 4.554 nm, were obtained for 2# film, while a relative higher Rmax

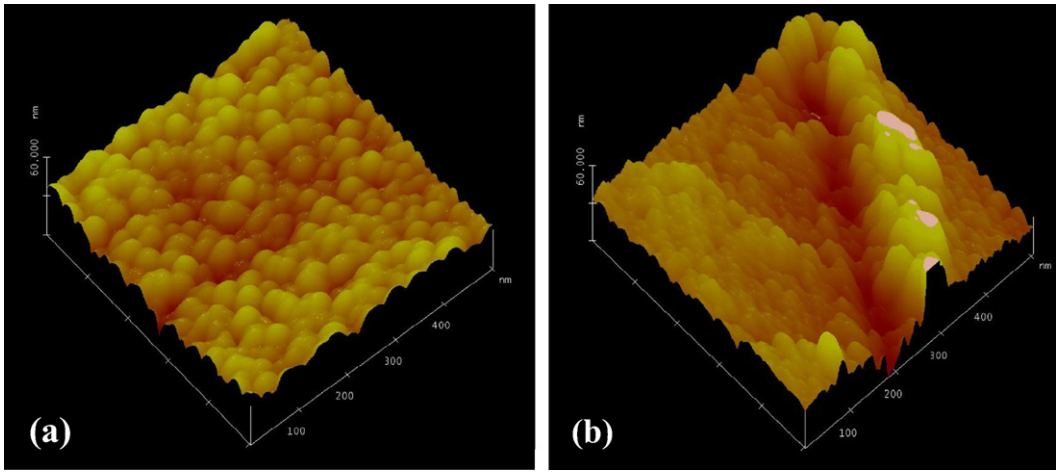

Fig. 4. AFM images of representative TiO_2 films. (a) 3D AFM image of 2# film. (b) 3D AFM image of 3# film.

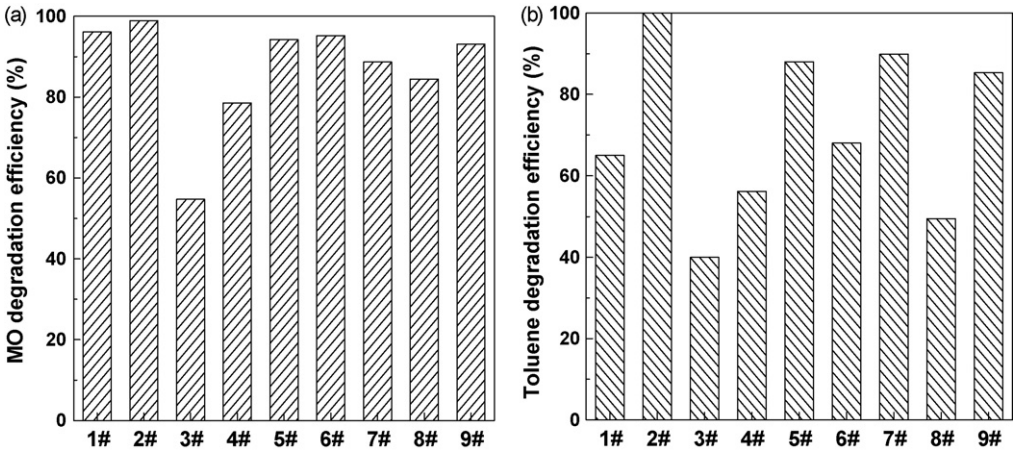

Fig. 5. Photocatalytic degradation efficiencies of TiO_2 films for (a) aqueous MO and (b) gaseous toluene.

of 86.426 nm, with Ra of 7.912 nm and Rms of 10.868 nm, was gotten for 3# film. The 3# film has much rough surface, which is readily favor the adsorption of organic pollutants. These results indicate that the films exhibiting different morphologies can be synthesized at different designed experiment conditions.

3.2. Photocatalytic activity of TiO_2 film

DOE and data analysis were used to optimize the affecting parameters for the preparation of a highly active photocatalyst. The photocatalytic activity of TiO_2 thin films strongly depends on the surface morphology and texture to some extent [30]. However, little work on the correlation of the photocatalytic activity and the morphology of the TiO_2 films has been reported. We have studied the photocatalytic activities of nine films prepared by DOE, and evaluated the degradation efficiencies of MO in solution and toluene in the gas. Fig. 5a shows the results of the photocatalytic degradation of MO in the presence of nine TiO_2 thin films prepared by DOE. The photocatalytic degradation efficiencies of MO within 1 h illumination are in range of 54.7–98.9%. The highest photocatalytic efficiency is 98.9% over 2# film, while the lowest photocatalytic efficiency is 54.7% over 3# film.

In addition, photocatalytic activities were also evaluated by measuring degradation efficiencies of gaseous toluene in the presence of nine prepared films. As shown in Fig. 5b, the photocatalytic degradation efficiencies within 1 h illumination are in range of 40.0–100% for nine prepared films. The changing tendency of the degradation efficiency over 1#–9# films is similar to that of the photocatalytic degradation of MO in solution (Fig. 5a). The highest photocatalytic efficiency of 100% and the lowest photocatalytic efficiency of 40.0% for the photocatalytic degradation of gaseous toluene were obtained over 2# film and 3# film, respectively. The difference in the photocatalytic activity of the synthesized samples is caused by different characteristic parameters of surface morphology. As mentioned before, XRD, FE-SEM and AFM results have shown that the 2# film consists of well-crystallized spherical nanoparticles with uniform surface, while the 3# film consists of incompact and asymmetry nanoparticles. However, the photocatalytic activities of the prepared films not only depend on the surface roughness of films, but also depend on the amount of loaded photocatalyst. The amount of loaded TiO_2 photocatalysts for 1#–9# films is 0.122, 0.211, 0.040, 0.057, 0.065, 0.105, 0.093, 0.047 and 0.033 mg/cm^2, respectively. The amount of photocatalyst of 2# film is highest (0.211 mg/cm^2) and the 3# film is lowest (0.004 mg/cm^2), respectively, resulting in the apparent difference in their photocatalytic activities.

3.3. Design of experiment and data analysis

As indicated by our results, the photocatalytic degradation efficiencies of aqueous MO and gaseous toluene depend on the film's surface morphology that can be controlled by the preparation recipe and preparation conditions in the sol–gel process. Therefore, the data analysis of DOE was employed to evaluate the effect of various preparation parameters on the photocatalytic activities of nine prepared films. According to the designed experimental conditions with L9 orthogonal array, the photocatalytic degradation efficiencies of MO in solution and toluene in the gas over nine prepared films are given in Table 2. The experimental results of DOE are first analyzed by using the direct observation analysis, because the responses versus the levels of different factors can be observed directly from a broken line plot [31]. The mean value of the degradation efficiencies for the corresponding factors at each level was calculated according to the assignment of the experiment. The corresponding diagrams of direct observation analysis for the individual effect of various parameters at each level are shown in Fig. 6. The difference between the maximal mean value and the minimum mean value for degradation efficiencies at each factor is defined as the extreme difference, which reflects direct effect of each factor. The larger of the extreme difference of mean value is, the more significant of controlling factors is. As shown in Fig. 6a and b, the extreme differences of four controlling factors both for the liquid-phase degradation of MO and the gas-phase degradation of toluene have an identical order: factor D > factor C > factor B > factor A. The calcination temperature (factor D) has significant influence on the photocatalytic activity. On the contrary, the volume of acetic acid aqueous solution (factor A) and alcohol (factor B) only play a minor role in controlling the photocatalytic performances.

Table 2
Assignment of L9 orthogonal array and the photocatalytic efficiencies.

Run no.	Factor A	Factor B	Factor C	Factor D	$y_{MO,\ average}$ (%)	$y_{toluene,\ average}$ (%)
1#	Level 1	Level 1	Level 1	Level 1	96.1	65.0
2#	Level 1	Level 2	Level 2	Level 2	98.9	100.0
3#	Level 1	Level 3	Level 3	Level 3	54.7	40.0
4#	Level 2	Level 1	Level 2	Level 3	78.6	56.2
5#	Level 2	Level 2	Level 3	Level 1	94.2	88.0
6#	Level 2	Level 3	Level 1	Level 2	95.2	68.0
7#	Level 3	Level 1	Level 3	Level 2	88.7	89.9
8#	Level 3	Level 2	Level 1	Level 3	84.5	49.5
9#	Level 3	Level 3	Level 2	Level 1	93.1	85.3

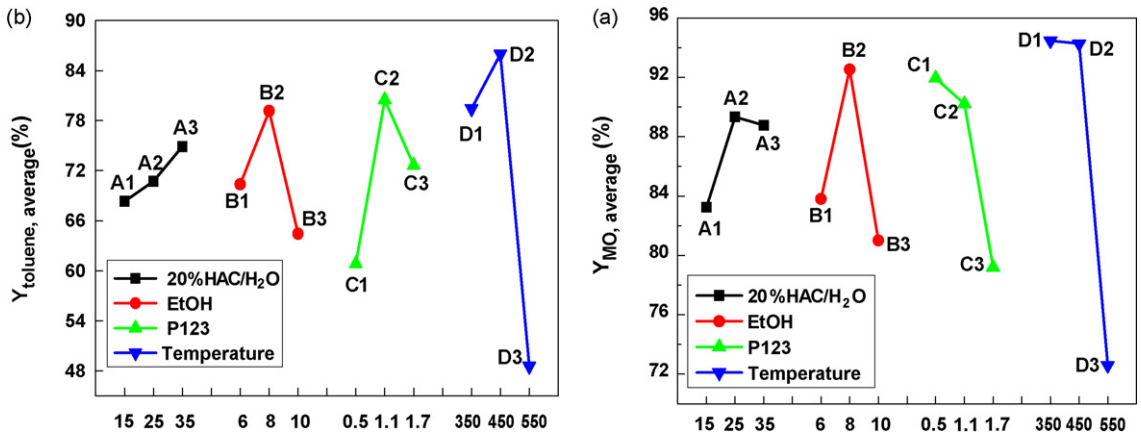

Fig. 6. The responding diagrams of direct observation analysis for individual effects of various parameters at different levels. (a) Photocatalytic degradation aqueous MO. (b) Photocatalytic degradation gaseous toluene.

Data analysis by analysis of variance (ANOVA) is much more scientific than the direct observation analysis [32]. Thus, ANOVA was also used to analyze the influence of various preparation parameters on the photocatalytic activity of nine prepared films. The effects of different factors on the response function were evaluated by calculating F value (variances ratio), to identify the importance of the factor in the DOE whenever the F value exceeds the critical points F ($F_{critical}$). Table 3 presents ANOVA results for photocatalytic degradation of MO in solution with a 90% confidence interval and toluene in gas with a 95% confidence interval, both at the degree of freedom value of 2. As for the MO photocatalytic degradation, the sum of square (68.15) of factor A at the volume of 20% acetic acid solution are much less than other three factors, and thus it can be treated as an error item. Moreover, the degree of free of error is 2, i.e., $f_e = f_A = 2$, and then the $F_{critical}$ (10%, 2, 2) was obtained as 9.0. Only the F value of 13.91 for factor D exceeds the $F_{critical}$, therefore we can conclude that the factor D (the calcination temperature) appears to be the significant contribution to the photocatalytic degradation efficiency of MO in solution. Also, it can be observed from Table 3 that the factor D is the most significant factor with 63.00% contribution. However, the factor A, at the volume of 20% acetic acid aqueous solution with 4.50% contribution, seems less significant than both factor B (the volume of alcohol, with 13.40% contribution) and factor C (the amount of P123, with 19.10% contribution). Thus, the order of the importance of four factors on the photocatalytic degradation of MO in solution is: factor D > factor C > factor B > factor A, which is the same as that obtained by the direct observation analysis.

For photocatalytic degradation of toluene, the sum of square of factor A (66.42) and factor B (329.72) are less than other two factors, factor C (587.90) and factor D (2394.20), and thus we consider both factor A and factor B as error items. So the degree of free of error was got as 4 in this system, i.e., $f_e = f_A + f_B = 4$. Known from Table 3, only F value of 12.09 for factor D (the calcination temperature) is larger than 6.94 for $F_{critical}$ (5%, 4, 2). It is noted that the factor D also has significant influence on the photocatalytic degradation gaseous toluene with 95% confidential interval. Similar result was also obtained from the data of percent contribution (%). The factor D has significant contribution with 70.87% confidential interval, which is by far higher than 17.40% for factor C, 9.76% for factor B, and 1.97% for factor A. Thus for photocatalytic degradation of gaseous toluene, the importance of four factors also has an order of factor D > factor C > factor B > factor A.

It is noteworthy that the optimal factors affecting the photocatalytic activity can be obtained by both direct observation analysis and ANOVA of experimental data. A favorable recipe should consider the balance between the photocatalytic performance and the reasonable selection of multiple variables based on economic and effectual viewpoint. Thus the optimal combination was obtained as A1, B2, C2 and D2, which is exactly the preparation recipe for the 2# film in the orthogonal array of Table 1. According to the above mentioned results, we can firmly conclude that our optimal combination condition for highly photocatalytic performance would be $Ti(OC_4H_9)_4$/20%HAC/EtOH/P123 = 2 g/15 ml/8.0 ml/1.1 g, and the calcination temperature of 450 °C.

Table 3
ANOVA of the efficiencies for photocatalytic degradation of aqueous MO and gaseous toluene.

Factor	Sum of square	Degree of freedom	Variance	F-test	Percent contribution (%)
MO					
A	68.15	(2)	34.08	1.00	4.50
B	201.66	2	100.83	2.96	13.40
C	286.14	2	143.07	4.20	19.10
D	947.64	2	473.82	13.91	63.00
Error	68.15	(2)	34.08		4.50
Total	1503.59	8	751.80		100
$F_{critical}$0.10 = 9.00					
Toluene					
A	66.42	(2)	33.21	0.34	1.97
B	329.72	(2)	164.86	1.67	9.76
C	587.90	2	293.95	2.97	17.40
D	2394.20	2	1197.10	12.09	70.87
Error	396.14	(4)	99.04		11.73
Total	3378.24	8	1689.12		100
$F_{critical}$0.05 = 6.94					

Acknowledgments

This is contribution No. IS-1073 from GIGCAS. The authors gratefully acknowledge the financial support from National Nature Science Foundation of China (40572173), the Science and Technology Project of Guangdong province, China (2007A032301002 and 2006A36701002) and The Combination Project of Production, Studying, and Research of Foshan City (2008A040 and 2006A015).

References

[1] L.F. Zhang, W.A. Anderson, S. Sawell, C. Moralejo, Chemosphere 68 (2007) 546–553.
[2] L.P. Yang, Z.Y. Liu, H.W. Shi, H. Hu, W.F. Shangguan, Catal. Today 126 (2007) 359–368.
[3] S.B. Kim, S.C. Hong, Appl. Catal. B-Environ. 35 (2002) 305–315.
[4] G.E. Imoberdorf, H.A. Irazoqui, A.E. Cassano, O.M. Alfano, Ind. Eng. Chem. Res. 44 (2005) 6075–6085.
[5] R. Taranto, D. Frochot, P. Pichat, Ind. Eng. Chem. Res. 46 (2007) 7611–7614.
[6] T.C. An, J.K. Liu, G.Y. Li, S.Q. Zhang, H.J. Zhao, X.Y. Zeng, G.Y. Sheng, J.M. Fu, Appl. Catal. A-Gen. 350 (2008) 237–243.
[7] S.N. Hosseini, S.M. Borghei, M. Vossoughi, N. Taghavinia, Appl. Catal. B-Environ. 74 (2007) 53–62.
[8] M.E. Osugi, G.A. Umbuzeiro, F.J.V. De Castro, M.V.B. Zanoni, J. Hazard. Mater. 137 (2006) 871–877.
[9] V. Subramanian, P.V. Kamat, E.E. Wolf, Ind. Eng. Chem. Res. 42 (2003) 2131–2138.
[10] Y. Liu, X. Wang, F. Yang, X. Yang, Micropor. Mesopor. Mater. 114 (2008) 431–439.
[11] P. Evans, D.W. Sheel, Surf. Coat. Technol. 201 (2007) 9319–9324.
[12] M.F. Hossain, S. Biswas, T. Takahashi, Y. Kubota, A. Fujishima, Thin Solid Films 516 (2008) 7149–7154.
[13] B. Yoo, K. Kim, S.H. Lee, W.M. Kim, N.-G. Park, Solar Energy Mater. Solar Cells 92 (2008) 873–877.
[14] I.D. Kim, A. Rothschild, D.J. Yang, H.L. Tuller, Sens. Actuators B-Chem. 130 (2008) 9–13.
[15] W.Y. Gan, M.W. Lee, R. Amal, H. Zhao, K. Chiang, J. Appl. Electrochem. 38 (2008) 703–712.
[16] T. Maekawa, K. Kurosaki, T. Tanaka, S. Yamanaka, Surf. Coat. Technol. 202 (2008) 3067–3071.
[17] K.O. Awitor, A. Rivaton, J.L. Gardette, A.J. Down, M.B. Johnson, Thin Solid Films 516 (2008) 2286–2291.
[18] A. Kleiman, A. Marquez, D.G. Lamas, Surf. Coat. Technol. 201 (2007) 6358–6362.
[19] S.K. Sharma, M. Vishwas, K.N. Rao, S. Mohan, D.S. Reddy, K.V.A. Gowda, J. Alloys Compd. 471 (2009) 244–247.
[20] L. Zhao, Y. Yu, L. Song, M. Ruan, X. Hu, A. Larbot, Appl. Catal. A-Gen. 263 (2004) 171–177.
[21] K.S. Liu, H.G. Fu, K.Y. Shi, F.S. Xiao, L.Q. Jing, B.F. Xin, J. Phys. Chem. B 109 (2005) 18719–18722.
[22] L. Zhang, Y.F. Zhu, Y. He, W. Li, H.B. Sun, Appl. Catal. B-Environ. 40 (2003) 287–292.
[23] J.K. Liu, T.C. An, G.Y. Li, X.Y. Zeng, N.Z. Bao, G.Y. Sheng, J.M. Fu, Micropor. Mesopor. Mater., in press.
[24] C.H. Wu, C.F. Wu, J.F. Shr, C.T. Hsieh, Sep. Purif. Technol. 61 (2008) 258–265.
[25] W.L. Yu, S.J. Wu, S.W. Shiah, Int. J. Hydrogen Energy 33 (2008) 2311–2322.
[26] Z.C. Wang, J.F. Chen, X.F. Hu, Mater. Lett. 43 (2000) 87–90.
[27] T.X. Liu, F.B. Li, X.Z. Li, J. Hazard. Mater. 152 (2008) 347–355.
[28] A. Verma, S.A. Agnihotry, Electrochim. Acta 52 (2007) 2701–2709.
[29] D.S. Tsoukleris, T. Maggos, C. Vassilakos, P. Falaras, Catal. Today 129 (2007) 96–101.
[30] Y. Saito, S. Kambe, T. Kitamura, Y. Wada, S. Yanagida, Solar Energy Mater. Solar Cells 83 (2004) 1–13.
[31] Y. Yamini, A. Saleh, M. Khajeh, Sep. Purif. Technol. 61 (2008) 109–114.
[32] G. Zhu, H. Ju, Anal. Chim. Acta 506 (2004) 177–181.